A non-linear system patterns Rab5 GTPase on the membrane

Cezanne A[1], Lauer J[1], Solomatina A[1,2,3], Sbalzarini IF[2,3,1] & Zerial M[1]

[1] Max-Planck Institute of Molecular Cell Biology and Genetics, Dresden, Germany
[2] Chair of Scientific Computing for Systems Biology, Faculty of Computer Science, TU Dresden, Germany
[3] MOSAIC Group, Center for Systems Biology Dresden, Germany

Abstract (146 words)

Proteins can self-organize into spatial patterns via non-linear dynamic interactions on cellular membranes. Modelling and simulations have shown that small GTPases can generate patterns by coupling guanine nucleotide exchange factors (GEF) to effector binding, generating a positive feedback of GTPase activation and membrane recruitment. Here, we reconstituted the patterning of the small GTPase Rab5 and its GEF/effector complex Rabex5/Rabaptin5 on supported lipid bilayers as a model system for membrane patterning. We show that there is a "handover" of Rab5 from Rabex5 to Rabaptin5 upon nucleotide exchange. A minimal system consisting of Rab5, RabGDI and a complex of full length Rabex5/Rabaptin5 was necessary to pattern Rab5 into membrane domains. Surprisingly, a lipid membrane composition mimicking that of the early endosome was required for Rab5 patterning. The prevalence of GEF/effector coupling in nature suggests a possible universal system for small GTPase patterning involving both protein and lipid interactions.

Introduction

Membrane compartmentalization is of central importance for a variety of biological functions at multiple scales, from sub-cellular structures to multi-cellular organisms. Processes such as cell polarization, protein and lipid sorting within sub-cellular organelles or cell and tissue morphogenesis depend on the emergence of patterns (Turing, 1952; Halatek *et al.*, 2018). In *Caenorhabditis elegans*, symmetry breaking of the plasma membrane is caused by PAR proteins that sort into distinct anterior and posterior cortical domains and generate cell polarity (Kemphues *et al.,* 1988, Motegi & Seydoux, 2013). In budding yeast, the site of bud formation is marked by a single, discrete domain of Cdc42 on the plasma membrane (PM) (Ayscough *et al.* 1997; Gulli *et al.* 2000; Irazoqui *et al.* 2003). In xylem cells, ROP11 is organized into multiple domains on the PM where it interacts with cortical microtubules to regulate cell wall architecture (Yang and Lavagi 2012; Oda and Fukuda 2012). Membrane compartmentalization is not limited to the plasma membrane but occurs also on cytoplasmic organelles. On early endosomes (EE), Rab5 exists in domains where it regulates vesicle tethering and fusion (McBride *et al.* 1999; Sönnichsen *et al.* 2000; Franke *et al.* 2019).

Cdc42, ROP11 and Rab5 are small GTPases, a class of molecules that play an important role in symmetry breaking and membrane compartmentalization. Small GTPases use GTP/GDP binding to act as an ON/OFF switch. The cycling between GTP and GDP-bound states is regulated by guanine nucleotide exchange factors (GEFs) and GTPase activating proteins (GAPs) (Bos *et al.* 2007; Cherfils and Zeghouf 2013). Most small GTPases are post-translationally modified by lipid chains which allow them to associate with membranes (Wang and Casey 2016). The inactive GTPase forms a high-affinity complex with guanine dissociation inhibitor (GDI), regulating membrane cycling (Sasaki *et al.* 1990; Ghomashchi *et al.* 1995; Cherfils and Zeghouf 2013). Nucleotide exchange prevents interaction with GDI and targets the GTPase to the membrane, where it can recruit effector proteins and mediate downstream activities (Wu *et al.* 2010; Langemeyer *et al.* 2018). Upon hydrolysis of GTP to GDP the GTPase is once again available for extraction from the membrane by GDI (Rak *et al.* 2004; Ghomashchi *et al.* 1995; Pylypenko *et al.* 2006).

It has been proposed that small GTPase patterning can arise from the coupling of GEF activity and effector binding (Horiuchi *et al.* 1997; Zerial and McBride, 2001). In this way, an active GTPase can recruit its own GEF, creating a local, positive feedback loop of GTPase activation and membrane recruitment. In general, self-organizing systems that form spatial patterns on

membranes often exhibit such non-linear dynamics of membrane recruitment and activation (Halatek *et al.*, 2018). The prevalence of GEF/effector coupling in small GTPase systems suggests that this may be a general mechanism for symmetry breaking & spatial organization of GTPases (Goryachev and Leda 2019). The Rab5 GEF, Rabex5 is found in complex with the Rab5 effector Rabaptin5. (Horiuchi *et al.* 1997). Similarly, the Cdc42 GEF Cdc24 is coupled to the effector Bem1 (Chenevert *et al.* 1992). Computational modelling revealed a Turing-type mechanism of pattern formation by a minimal system composed of Cdc42, the Bem1/Cdc24 complex and GDI (Goryachev and Pokhilko 2008; Goryachev and Leda 2017). In plants, the ROP11 GEF, ROPGEF4, forms a dimer that catalyzes nucleotide exchange but also interacts with the active ROP11 (Nagashima *et al.* 2018). We focus on Rab5, its GEF/effector complex Rabex5/Rabaptin5, and RabGDI (hereafter referred to as GDI) in order to investigate general mechanisms for the spatial organization of peripheral membrane proteins.

Rabex5/Rabaptin5 is one of the best characterized GEF/effector complexes in eukaryotes. Rabex5 is a 57kDa Vps9 domain containing GEF for Rab5 (Horiuchi *et al.* 1997; Delprato and Lambright 2007; Lauer *et al.*, 2019). Rabaptin5 is a 99kDa protein with multiple protein-protein interaction sites that colocalizes with Rab5 on EE and is essential for endosome fusion (Stenmark *et al.* 1995; Horiuchi *et al.* 1997). Due to the dimerization of Rabaptin5, the complex is a tetramer (Lauer *et al.*, 2019). The interaction with Rabaptin5 has been shown to increase Rabex5 GEF activity and produce structural rearrangements in Rabex5 (Delprato *et al.* 2004; Delprato and Lambright 2007; Lippe *et al.* 2001; Horiuchi *et al.* 1997; Zhang *et al.* 2014, Lauer *et al.*, 2019). By binding active Rab5, Rabaptin5 localizes the enhanced GEF activity of Rabex5 in the vicinity of active Rab5, thereby creating the positive feedback loop. In addition, Rabex5 can be recruited to EE via binding to Ubiquitin via two distinct Ubiquitin binding domains near the N-terminus (Penengo *et al.,* 2008). Interestingly, Ubiquitin binding enhances GEF activity toward Rab5 helping to initiate the positive feedback loop on endosomes carrying ubiquitinated cargo (Lauer *et al.*, 2019). Blümer *et al.* (2013) observed that artificially targeting Rabex5 to mitochondria resulted in Rab5 recruitment to these organelles, suggesting that Rabex5 can be sufficient for localizing Rab5 to a membrane compartment. Rab5 associates with the membrane by two 20-carbon geranylgeranyl chains attached at the C-terminus of the protein (Farnsworth *et al.* 1994). Molecular dynamics simulations showed that both cholesterol and PI(3)P accumulate in the vicinity of Rab5, and predicted a direct interaction with PI(3)P mediated by an Arg located in the flexible hypervariable region (HVR) between the C-terminal lipidation and the conserved GTPase domain (Edler *et al.* 2017).

Elucidating the precise mechanisms of self-organization of peripheral membrane proteins is critical to understanding endomembrane identity and functionality. We hypothesize that, similar to what has been observed for Cdc42 *in silico*, Rab5, Rabex5/Rabaptin5 and GDI comprise a minimal system that is capable of spatially organizing Rab5. We made use of *in vitro* reconstitution to test this hypothesis and elucidate the contributions of individual components to membrane association and organization. Our biochemical reconstitution system allowed for in-depth study of the biochemical interactions underlying the self-organization of Rab5 and its interacting molecules on the membrane.

Results

Upon GDP/GTP exchange Rab5 is directly transferred from Rabex5 to Rabaptin5 - a mechanistic basis for positive feedback of Rab5 activation

To directly test the positive feedback loop model, we investigated the structural rearrangements occurring in Rab5 and Rabex5/Rabaptin5 in the course of nucleotide exchange by Hydrogen Deuterium Exchange Mass Spectrometry (HDX-MS). Rabex5/Rabaptin5 was first premixed with Rab5:GDP and the resulting ternary complex diluted into deuterated buffer in the absence (Figure 1A top) or presence (Figure 1A bottom) of GTP□S and incubated for 1, 5 and 15 min. In this way, we could monitor structural rearrangement occurring in the early stages of the nucleotide exchange reaction. Focusing first on Rab5, we could see evidence of nucleotide exchange from the dramatic stabilization of Val24-Leu38, Leu130-Leu137 and Met160-Met168, encompassing the P-loop and parts of □5, α4 and □6 (Figure 1 B: dark blue), which, together, make up most of the direct interaction sites with GTP. In addition, we saw stabilization of Gln60-Phe71, parts of □2 and □3 (sky blue and pale green), consistent with the binding of Rabaptin5 (Zhu et al., 2004). Indication of binding to Rabaptin5 was observed after only 1 minute of reaction, thus providing evidence of a direct hand-off of active Rab5 from the Rabex5 catalytic domain to Rabaptin5 (See Figure 1 C). Interestingly, we also saw a destabilization of Ile177-Asp200, α5 (yellow), suggesting a structural rearrangement of the C-terminal HVR. Figure 1 D shows the alterations in deuterium exchange for Rabaptin5. Since there is no available structural model for Rabaptin5 the data are represented as a graph in which each peptide showing statistically significant alterations in deuterium uptake is assigned a value for the percent alteration. We saw stabilization in both of the regions known to bind Rab5, thus providing further evidence of Rab5 binding to Rabaptin5 after the nucleotide exchange reaction.

This provides a putative structural mechanism for positive feedback loop formation and the need to couple GEF and effector activities. Next, we set out to test the hypothesis that such positive feedback is sufficient to induce the recruitment and localized accumulation of membrane-bound Rab5.

Reconstituting Rab5 domain formation *in vitro*

To reconstitute Rab5 membrane recruitment and organization, we developed an *in vitro* system consisting of recombinant proteins and synthetic membranes. The lipid composition of the synthetic membrane was chosen based on the lipid composition of an enriched early endosomal fraction from HeLa cells characterized by mass spectrometry in a previous study (Perini, 2012). Lipids constituting over 1mol% of this lipid composition were utilized (EE, See Table S1). In order to test a wide number of experimental conditions, we designed the following workflow: small unilamellar vesicles with the EE-like lipid composition (EE-SUV) were deposited onto 10µm silica beads to form membrane-coated beads (EE-MCB). EE-MCBs were incubated with recombinant proteins, some of which were fluorescently tagged allowing us to monitor protein recruitment and spatial organization using confocal microscopy. EE-MCBs were segmented and visualized as Mollweide map projections as described in Solomatina *et al.* (submitted, 2019). For visualization, the EE-MCBs are presented as equatorial slices in GFP/RFP and DiD channels, and the reconstructed bead surface as a Mollweide map projection of the GFP/RFP signal (Mollweide map projections of the DiD signal can be found in the corresponding supplementary figures).

EE-MCBs incubated with 10nM GFP-Rab5/GDI showed membrane recruitment of GFP-Rab5 with a random distribution (see Figure 2 A). The addition of 1µM GDI and Rabex5/Rabaptin5-RFP in the presence GDP removed GFP-Rab5 from the membrane (see Figure 2 B). However, the same reaction in the presence of GTP produced a striking redistribution of GFP-Rab5 on the membrane into discrete clusters or domains (see Figure 2 C and Supplemental Video 1). Interestingly, the formation of GFP-Rab5 domains required GDI in a concentration-dependent manner (see Figure 2 D-F). GFP-Rab5 domains were segmented using Squassh (Rizk *et al.* 2014; Solomatina *et al.* submitted 2019) on the surface of the bead, and the segmented structures were then characterized in terms of size and fluorescence intensity. Table 1 summarizes the characteristics of GFP-Rab5 domains from experiments shown in Figure 2, 3 and 6. Domains with a mean diameter of 1.32µm were detected on MCBs incubated with GFP-Rab5/GDI, GDI, Rabex5/Rabaptin5, and GTP but not GDP. They formed with a characteristic

density of ~4.7 domains/EE-MCB and were rarely found adjacent to one another. A critical hallmark of the reconstituted domains is a marked increase in GFP-Rab5 signal within the segmented domain as compared to the area outside (See Figure 2 G). Comparison between GFP-Rab5 and DiD signals revealed that the occasional apparent clusters of GFP-Rab5 in the absence of other factors (see Figure 2 A) were due to membrane inhomogeneity characterized by lower DiD signal, unlike GFP-Rab5 domains.

In order to understand how these domains form, we monitored EE-MCBs over time (See Figure 2 H, Supplemental Video 2). Domains appear to be nucleated within the first minute of the reaction (which we could not capture due to the imaging setup) and then grow linearly in intensity until ~5 minutes after initiation of the reaction. After this point individual domains increase in GFP-Rab5 signal intensity slowly or not at all, suggesting that some domains reach saturation. Interestingly, domains recovered in the same locations after photobleaching indicating that there is a constant exchange of GFP-Rab5 with solution (See Figure 2 I, Supplemental Video 3).

Rabex5/Rabaptin5 is essential for Rab5 domain formation *in vitro*

In order to understand the mechanisms by which Rab5 domains form, we dissected the contribution of each component of our reconstituted system. GDI delivers and extracts Rab5, as seen in Figure 2, and is essential for domain formation. We observed that, similar to GDI, Rab5 domain formation requires Rabex5/Rabaptin5 in a concentration-dependent manner (see Figure 3 A-E and Table 2, which summarizes the conditions shown in Figure 3 A, B & C).

Next, we verified that the Rabex5/Rabaptin5 complex indeed localizes to the Rab5 domain. For this, we used a fluorescent Rabex5/Rabaptin5-RFP complex and observed both enrichment of Rabaptin5-RFP signal inside the domain (See Figure 4 A) and colocalization with GFP-Rab5 (See Figure 4 B). Rabex5/Rabaptin5-RFP also showed some degree of membrane association in the absence of other factors (See Figure S3 F), however this was significantly lower than the signal observed inside the GFP-Rab5 domains.

We next wanted to investigate whether the full Rabex5/Rabaptin5 complex was necessary for domain formation (Figure 3 F-J). In the presence of Rab5, GDI and GTP, neither full-length Rabex5 nor the Rabex5 catalytic domain (Rabex5CAT) alone were sufficient to form domains (Figure 3 F, G). Similarly, Rabaptin5 alone was not capable of forming domains (Figure 3 H). Unlike the full length Rabex5/Rabaptin5 complex, Rabex5CAT plus full-length Rabaptin5 did

not support Rab5 domain formation (compare Figure 3 J and I). This suggests that direct coupling of GEF activity and effector binding is essential for Rab5 domain formation.

Finally, we quantified the domain size distribution as a function of concentration of the components in the reaction. Interestingly, neither the domain diameter nor the area differed significantly when decreasing Rabex5/Rabaptin5 concentration, but the mean intensity of domains decreased with decreasing concentration of Rabex5/Rabaptin5 (See Figure 3 E and Table 2).

Rab5 domain formation is influenced by membrane composition

In addition to protein-protein interactions, protein-lipid and lipid-lipid interactions also play a role in Rab5 domain formation. The above experiments (Figures 2 and 3) were all conducted with the EE lipid composition containing 1mol% PI(3)P. The rearrangements in Rab5 during nucleotide exchange reveal a destabilization of α5 that may alter membrane contacts or orientation of the protein with respect to the membrane in the GDP- vs GTP-bound conformation (See Figure 1 B). Previous work using molecular dynamics simulations suggested an interaction between the Rab5 HVR and PI(3)P as well as cholesterol (Edler *et al.* 2017). To investigate the contribution of lipids, specifically PI(3)P and cholesterol, to GFP-Rab5 domain formation, EE-MCBs as well as MCBs with a simple PC/PS lipid composition were made with either 1mol% or 0mol% PI(3)P (PC/PS-MCB; See Table S1). Geranylgeranylated GFP-Rab5 was recruited similarly to EE-MCBs and PC/PS-MCBs that included 1mol% PI(3)P (see Figure 5 A, B & E). However, recruitment of GFP-Rab5 to both membranes lacking PI(3)P was greatly diminished (see Figure 5 C-E). This suggests that the presence of PI(3)P enhances Rab5 recruitment, either by facilitating the dissociation of Rab5 from GDI or by inhibiting the extraction of Rab5 by GDI. The presence of cholesterol appeared to also improve Rab5 recruitment to the simple lipid composition, although to a lesser degree than PI(3)P (See Figure 5 F; PC/PS/CH-MCB vs PC/PS-MCB, See Table S1). Investigation of the contribution of cholesterol in the EE-like lipid composition was not possible in this system as membrane integrity was greatly compromised without cholesterol (data not shown).

In order to determine whether these interactions have an effect on domain formation, the same MCBs were incubated with Rab5/GDI, Rabex5/Rabaptin5, GDI and GTP. Strikingly, domain formation was most efficient on EE-MCBs with 1mol% PI(3)P, less efficient on EE-MCBs with 0mol% PI(3)P and completely abolished on PC/PS membranes regardless of PI(3)P content (see Figure 6 and Table 3 which summarizes the conditions shown in Figure 6).

Domains formed on EE membranes in the absence of PI(3)P had a drastically reduced mean domain intensity (508.32 ± 143.37) compared to domains formed in the presence of PI(3)P (mean domain intensity 1269.32 ± 556.54) (See Figure 6 E). Importantly, the membrane association of Rabex5/Rabaptin5-RFP was not found to be similarly lipid composition-dependent (See Figure S3 F). The observation that Rab5 can be recruited efficiently to PC/PS/PI(3)P membranes but cannot be organized into domains in the presence of Rabex5/Rabaptin5, excess GDI, and GTP suggest that Rab5 interacts differently with the complex EE membrane that with a simple PC/PS membrane. Our results demonstrate that PI(3)P enhances recruitment of Rab5 to MCBs and the presence of lipids mimicking the content of the early endosome helps drive Rab5 domain formation.

Discussion

GEF/effector coupling and the resulting positive feedback loop of GTPase activation and membrane recruitment are common to many small GTPase systems and have been implicated in their spatial patterning. In this study, we demonstrated that membrane recruitment and extraction (via GDI) together with coupling of GEF and effector activities (via Rabex5/Rabaptin5) are sufficient to reconstitute domain organization of Rab5 *in vitro*. Geranylgeranylated Rab5 was observed to be recruited to EE-like membranes from the Rab5/GDI complex. Whereas in the absence of other factors Rab5 was randomly distributed in the plane of the membrane, upon the addition of GDI, Rabex5/Rabaptin5 and GTP, it reorganized into discrete domains in a GTP-dependent manner. Key to Rab5 domain formation was the "handover" of Rab5 from Rabex5 to Rabaptin5 and the lipid composition of early endosomes, suggesting a hitherto unknown cooperativity between lipids and Rab-dependent membrane self-organization.

Self-organizing systems that form spatial patterns on membranes often depend on non-linear dynamics (Halatek et al., 2018). In our system, a key feature is the membrane recruitment and activation of Rab5, regulated by the Rabex5/Rabaptin5 complex. Neither GEF activity nor effector binding alone were capable of supporting domain formation unless physically coupled in a complex. We found that, in the course of nucleotide exchange, newly activated Rab5 is released from Rabex5 and immediately binds Rabaptin5 suggesting there is a direct delivery or "handover" of Rab5 from Rabex5 to Rabaptin5. This "handover" is likely facilitated by the dimerization of the Rabex5/Rabaptin5 complex and presents a structural mechanism by which

a positive feedback loop of Rab5 activation could be generated. Other Rab5 GEFs that localize and recruit Rab5 to different intracellular compartments (e.g. GAPVD1 or RIN1 on clathrin-coated vesicles and the plasma membrane; Tall *et al.* 2001; Semerdjieva *et al.* 2008) have as of yet not been found to be coupled to effector activity. *In vivo* Rabex5/Rabaptin5 can be targeted to the EE by interaction of Rabex5 with ubiquitinated receptors and the binding of Ubiquitin to Rabex5 enhances nucleotide exchange activity (Lee *et al.* 2006; Mattera *et al.* 2006; Penengo *et al.* 2006; Lauer *et al.,* 2019). This implies that ubiquitinated cargo can act not only to recruit Rabex5/Rabaptin5 but also potentially contribute to Rab5 domain formation and/or localization on the EE.

An important new finding of this study is the role of lipids in Rab5 domain formation. In our reconstituted system, PI(3)P and cholesterol enhanced the membrane recruitment of Rab5. In molecular dynamics simulations, Edler and Stein (2017b) suggest a direct interaction between Rab5 and PI(3)P and also observed accumulation of cholesterol in the proximity of Rab5. Lebrand *et al.* (2002) reported that cholesterol regulates the membrane association and activity of Rab7 on late endosomes *in vivo* and decreases GDI extraction of Rab7 *in vitro*. We therefore suggest that the presence of cholesterol is important for stabilizing Rab5 on the membrane by locally altering lipid packing to adapt to the longer chain length of the geranylgeranyl anchor. However, unlike Rab5 recruitment, domain formation was only observed on membranes containing the full EE lipid mixture. The observation that simple, highly diffusive, PC/PS membranes do not support domain formation suggests that the EE lipid composition facilitates lateral lipid packing and protein-lipid interactions that are necessary for domain formation. The destabilization of α5, which extends into the HVR, observed in Rab5 by HDX-MS may alter the conformation of membrane-bound Rab5 upon nucleotide exchange. In molecular dynamics simulations, Edler and Stein (2017a) observed a rotation within the membrane of Rab5:GTP with respect to Rab5:GDP, that not only exposes the effector binding site but also suggests that Rab5 makes different membrane contacts depending on its nucleotide state. Further molecular dynamics simulations showed that this nucleotide state-dependent orientation, as well as correct insertion of the geranylgeranyl anchors into the lipid bilayer, is only supported by an EE-like membrane, containing PI(3)P, cholesterol, and charged lipids (Edler and Stein 2017a; Münzberg and Stein, 2019). We suggest that the EE lipid composition supports Rab5 domain formation in our *in vitro* system through a combination of 1) direct interactions between Rab5 and PI(3)P, 2) cholesterol stabilizing the geranylgeranyl anchor insertions and 3) the presence of charged lipids allowing for interactions between Rab5 and lipid headgroups that support the nucleotide-dependent orientation of Rab5 relative to the membrane. Unfortunately, technical

limitations did not allow us to investigate domain formation on membranes that lack lipids from the EE composition (e.g. cholesterol, sphingomyelin, GM3 or charged lipids) as MCBs became unstable with these lipid compositions.

The non-linearity of the nucleotide cycle coupled to specific lipid interactions make small GTPases widespread regulators of membrane self-organization. K-Ras for example, has long been known to cluster and alter the local lipid environment, e.g. by forming nanoclusters of $PI(4,5)P_2$ on the PM (Zhou *et al.* 2017). However, with the same design, different GTPase systems can form one (e.g. Cdc42) or multiple domains (e.g. ROP11, Rab5). Our *in vitro* system recapitulates the formation of multiple Rab5 domains on the same membrane. In the reconstituted system, Rab5 domains were formed with a characteristic density of ~4.7 domains/EE-MCB surface and a mean diameter of 1.32µm. Chiou *et al.* (2018) propose that coexistence of multiple GTPase domains can arise if the density of active GTPase in the domain reaches a "saturation" point. This would slow competition between domains, allowing multiple domains to exist simultaneously, and could occur via multiple biologically relevant mechanisms (e.g. local depletion of components or strong negative feedback). In our reconstituted system, we indeed saw both characteristic spacing of domains and saturation of GFP-Rab5 signal, indicating that such a "saturation" point can be reached. From the domain intensity we could observe two phases in domain growth, an initial phase characterized by rapid increase in GFP signal intensity over time, and a second phase characterized by slow increase or even saturation in signal intensity. We suggest that fast growth is dominated by reorganization of the local lipid environment and rapid recruitment of proteins from solution. Upon depletion of the critical components from the local membrane, domains stabilize and reach a second, slow-growing or saturated phase. We suggest that in this phase, domains reach dynamic equilibrium where domain size has stabilized but the domain continues to exchange proteins with the soluble pool, as suggested by the observation that domains recover in the same location after photobleaching. It may therefore be the interaction with the lipid membrane that stabilizes and determines the size of the domains obtained in our system. Further, it is apparent during purification that recombinant Rab5 dimerizes at high concentrations and this dimerization is enhanced by geranylgeranylation (data not shown). Given that domains create a locally high concentration of protein, Rab5 dimerization may also contribute to stabilization of a Rab5 domain. How domain growth is regulated and by what means biological systems can produce a variety of spatial patterns based on common design principles has been the subject of multiple recent *in silico* models and simulations (Chiou *et al.* 2018; Halatek *et al.*, 2018;

Jacobs *et al.* 2019). Our results imply that the specific interaction of proteins with lipids in the membrane must also be considered in such studies.

Herein, we reconstituted a minimal system for the formation of Rab5 GTPase domains *in vitro* and demonstrated that both GEF/effector coupling and lipid interactions contribute to the self-organization of Rab5 on the membrane, where the lipid composition plays an important role beyond that of a solvent for lipidated proteins. This appears to be a universal system deploying small GTPases to pattern membranes from mono-cellular to multi-cellular organisms.

Materials & Methods

Cloning

Rab5, Rabex5, Rabaptin5, and GDI were cloned into pOEM series vectors (Oxford Expression Technologies), modified to contain a Human Rhino Virus (HRV) 3C cleavable tag at either the Nor C-terminus, followed by a protease cleavage site (Not1 at N-terminus, Asc1 at C-terminus) for insect (SF9) cell expression. Cleavable tags consisted of either 6x-Histidine (6xHis), for Rab5 and Rabex5, or Gluthathione S-Transferase (GST), for GDI and Rabaptin5. In order to monitor membrane association and organization, fluorescent Rab5 and Rabaptin5 constructs were created. The proteins were cloned into SF9 expression vectors containing either an N or C-terminal fluorescent tag (GFP or RFP) attached to the protein by a 13 amino acid flexible linker (N-terminal linker: GSAGSAAGSGAAA; C-terminal: linker: GAPGSAGSAAGSG). As the addition of a fluorescent tag to a protein always carries the risk of altering protein behavior by interfering with protein folding, fluorescent proteins were compared to non-fluorescent constructs known to fold properly by Hydrogen Deuterium Exchange Mass Spectrometry (HDX-MS) and discarded if they showed any aberrant dynamics. The following constructs were used in this study: 6xHis-GFP-Rab5, GST-GDI, GST-Rabaptin5, Rabex5-6xHis, RFP-Rabaptin5, 6xHis-RabexCAT.

Protein Expression and Purification

SF9 cells were grown in ESF921 media (Expression Systems) and co-transfected with linearised viral genome and expression plasmid. P1 and P2 virus was generated per manufacturers protocol and yield was optimised by expression screens and infection time course experiments. The P2 virus was used to infect SF9 cells (grown to a density of 1 million cells/ml) at 1% (v/v). Rabex5/Rabaptin5 and geranylgeranylatedRab5/GDI complexes were produced by co-infection. Cells were harvested after 30-40hrs by spinning in a tabletop centrifuge at 500g for 10 minutes. Cell pellets were resuspended in Standard Buffer (20 mM Tris pH7.5, 150 mM NaCl, 5mM MgCl2, 0.5 mM TCEP; STD) supplemented with DNAse 1 and protease inhibitor cocktail (chymostatin 6 µg/mL, leupeptin 0.5 µg/mL, antipain-HCl 10 µg/mL, aprotinin 2 µg/mL, pepstatin 0.7 µg/mL, APMSF 10 µg/mL). Pellets were flash frozen and stored at -80°C. All subsequent steps performed at 4°C or on ice. Cells were thawed on ice and lysed by sonication (previously frozen SF9 cell pellets were not sonicated as freeze-thawing is sufficient for lysis). Cell lysates were spun with a JA 25.50 rotor at 22500rpm for 20 minutes at 4°C. Histidine-tagged proteins were bound to Ni-NTA Agarose resin (1L of culture = 1mL

resin) in the presence of 20mM Imidazole. Resin was washed with STD buffer supplemented with 20mM Imidazole. Proteins were eluted using 200mM Imidazole only followed by Histidine-tag cleavage during overnight dialysis with 3C protease. GST tagged proteins were bound to Glutathione Sepharose resin (GS-4B, GE Healthcare) for 2 hours at 4°C, washed with Standard Buffer and cleaved from resin overnight with a GST-3C protease. Rabex5/Rabaptin5 and Rab5/GDI complexes were purified by both His- and GST-tag affinity purification to obtain pure complex. Size Exclusion Chromatography was performed in STD on a Superdex200 Increase 10/30. Concentrations were determined by a bicinchoninic acid protein Assay (Pierce™ BCA Protein Assay Kit, ThermoFischer) and purity was assessed by SDS-PAGE followed by colloidal Coomassie staining. Proteins were aliquoted, flash frozen in liquid nitrogen and stored at -80°C.

Liposome preparation

The lipids listed below were purchased and resuspended in either CHCl3, CHCl3:MeOH (2:1 for GM3) or CHCl3:MeOH:H2O (1:2:0.8 for PI(3)P) as per manufacturer's instructions and stored at -20°C. To form liposomes, lipids were mixed together and the solvent was evaporated under a stream of nitrogen. Residual solvent was removed by drying under vacuum overnight in a desiccator. Lipids were rehydrated for at 37°C in SLB Buffer (20mM TRIS, 150mM NaCl) and vortexed to form a stock solution of 1mM lipid. Small unilamellar vesicles (SUV) were prepared by freeze-thaw cycles (10x snap freezing and thawing at 37°C). Vesicles were stored at -20°C and sized by sonication before each application. Size distribution of liposome preparations was assessed by Dynamic Light Scattering using a Zetasizer Nano ZSP Malvern.

EE lipid composition: DOPC(1,2-dioleoyl-sn-glycero-3-phosphocholine):DOPS(1,2-dioleoyl-sn-glycero-3-phospho-L-serine):DOPE(1,2-dioleoyl-sn-glycero-3-phosphoethanolamine):Sphingomyelin:Cholesterol:Plasmalogen PE (1-(1Z-octadecenyl)-2-oleoyl-sn-glycero-3-phosphoethanolamine):Plasmalogen PC (1-(1Z-octadecenyl)-2-oleoyl-sn-glycero-3-phosphocholine):GM3: PI(3P) (diC16 Phosphatidylinositol 3-phosphate): DiD [DiIC18(5); 1,1'-dioctadecyl-3,3,3',3'-tetramethylindodicar-bocyanine, 4-chlorobenzenesulfonate salt] (13.8:6.1:6.8:12.6:32.3:12.9:3.6:9:1:0.1) (See Table **S1**)

PC/PS lipid composition: DOPC(1,2-dioleoyl-sn-glycero-3-phosphocholine): DOPS(1,2-dioleoyl-sn-glycero-3-phospho-L-serine): Phosphatidylinositol 3-phosphate (PI(3P)diC16): DiD [DiIC18(5); 1,1'-dioctadecyl-3,3,3',3'-tetramethylindodicar-bocyanine, 4-chlorobenzenesulfonate salt] (83.95:15:1:0.1) (See Table **S1**)

MCB preparation

Silica beads (10µm standard microspheres for microscopy) were coated with a supported lipid bilayer as described (Neumann *et al.* 2013) with minor modifications to ensure a tight lipid membrane. Beads were incubated with either 800mM NaCl and 250µM EE liposomes or 375µM PC/PS liposomes (Z average diameter 100-120nm by SLS) for 15 minutes RT on a rotator wheel. MCBs were washed with 1ml H20 and 2x 1mL Standard Buffer, centrifuging at 2000rpm for 1 minute in a tabletop centrifuge. Membrane integrity was assessed at different time points and after increasing centrifugation steps. MCBs were found to be robust at 13000rpm washing steps and up to 4hrs at RT. MCBs were consequently used within 3hrs of formation. The formation protocol was adapted for PC/PS membranes in order to produce

MCBs with similar amounts of membrane as compared to EE-MCBs in order to make direct comparisons of GFP-Rab5 recruitment.

Confocal microscopy

Microscopy experiments were performed on either Nikon TiE (manual imaging, for high resolution and 3D reconstructions) or Cell Voyager 7000S (CV7000S) (automated imaging for time lapse experiments). For manual imaging in Nikon TiE, reactions were prepared in an 8-well Nunc^{TM} Lab-Tek^{TM} Chamber Slide for imaging. Images were acquired with a Nikon TiE equipped with a 100x/1.45NA Plan Apochromat, DIC oil immersion objective, Yokogawa CSU-X1 scan head and Andor DU-897 back-illuminated CCD. Images were acquired with 80ms exposure at λ 488, 561 and 660 with the following laser intensities: 15% 488; 5% 561; and 2% 660. For automated imaging, reactions were prepared in a Greiner Square bottom 384 well plate. Images were acquired with Cell Voyager 7000S (CV7000S) equipped with a 60x/1.2NA water immersion objective at 30% 488 and 660 laser. Color and illumination corrections were applied though CV7000S software. Imaging support by M. Stöter (TDS, MPI-CBG).

Image Analysis

Intensity quantifications at MCB equators were performed manually in FIJI (Schindelin *et al.,* 2012). Beads were segmented manually and intensity values along the surface were extracted by determining line profiles 10 pixels wide along the surface of the bead as defined by DiD signal. Intensity in 488 and 561 was normalized to the intensity in the 660 channel in a pixelwise manner to account for potential differences in membrane amount between beads and lipid compositions. Box and whiskers plots show median (line), 25/75 quartiles (box boundaries), and min/max values (error bars). Unpaired t-tests were performed to test statistical significance. Image analysis and visualization of MCBs was conducted as described by Solomatina *et al.* (submitted, 2019). Briefly the pipeline consists of (a) detection of spheres/beads in the image and reconstruction of the bead surface as a narrow band of particles, moment-conserving interpolation of the intensity values from the pixels to the particles, and radial maximum-intensity projection of the interpolated intensity values of the particles onto the exact surface of the sphere; (b) background subtraction on the bead surface using a "rolling ball" algorithm in the tangent space of the sphere (Sternberg, 1983); (c) segmentation of domains on the sphere using Squassh (Rizk *et al.* 2014); (d) radial projection of the segmented 3D structures onto the bead surface for effective size estimation; (e) visualization of the bead surface as a Mollweide map (Snyder, 1987); (f) statistical analysis of the sizes, intensities, spatial correlation analysis for multi-channel images.

Spatial representation of correlation

Correlation maps were created by computing the normalized mean deviation product (*nMDP*) as a measure of correlation between the corresponding pair of particles with intensities according to the formula:

$$nMDP = \frac{(A_i - \bar{A})(B_i - \bar{B})}{(A_{max} - \bar{A})(B_{max} - \bar{B})}$$

A_i and B_i – intensity of the given particle on the bead *A* or bead *B*
$\bar{A}$ and $\bar{B}$ – average intensity of the bead *A* or bead *B*
A_{max} and B_{max} – maximum intensity of the bead *A* or bead *B*

Hydrogen Deuterium Exchange-Mass Spectrometry (HDX-MS)

HDX-MS was performed essentially as previously described (He, Bai et al., 2015, Mayne, Kan et al., 2011, Walters, Ricciuti et al., 2012). Proteins (1 uM) are diluted 6:4 with 8M urea, 1% trifluoroacetic acid, passed over an immobilized pepsin column (2.1 mm x 30 mm, ThermoFisher Scientific) in 0.1% trifluoroacetic acid at 15 ˚C. Peptides are captured on a reversed-phase C8 cartridge, desalted and separated by a Zorbax 300SB-C18 column (Agilent) at 1 ˚C using a 5-40% acetonitrile gradient containing 0.1% formic acid over 10 min and electrosprayed directly into an Orbitrap mass spectrometer (LTQ-Orbitrap XL, ThermoFisher Scientific) with a T-piece split flow setup (1:400). Data were collected in profile mode with source parameters: spray voltage 3.4kV, capillary voltage 40V, tube lens 170V, capillary temperature 170 ˚C. MS/MS CID fragment ions were detected in centroid mode with an AGC target value of 10^4. CID fragmentation was 35% normalized collision energy (NCE) for 30 ms at Q of 0.25. HCD fragmentation NCE was 35eV. Peptides were identified using Mascot (Matrix Science) and manually verified to remove ambiguous peptides. For measurement of deuterium uptake, 10uM protein is diluted 1:9 in Rab5 buffer prepared with deuterated solvent. Samples were incubated for varying times at 22 ˚C followed by the aforementioned digestion, desalting, separation and mass spectrometry steps. The intensity weighted average m/z value of a peptide's isotopic envelope is compared plus and minus deuteration using the HDX workbench software platform. Individual peptides are verified by manual inspection. Data are visualized using Pymol. Deuterium uptake is normalized for back-exchange when necessary by comparing deuterium uptake to a sample incubated in 6M urea in deuterated buffer for 12-18h at room temperature and processed as indicated above.

Acknowledgements

We warmly thank David H. Murray for training in lipid techniques, discussions and support during the initial stages of the project. We also thank Yannis Kalaidzidis and Stephan Grill for their helpful discussions and suggestions, as well as Martin Stöter for help with the timelapse imaging. We would also like to thank the following Services and Facilities of the Max Planck Institute of Molecular Cell Biology and Genetics for their support: Light Microscopy Facility (LMF), Technology Development Studio (TDS) and the Protein Expression Purification and Characterization (PEPC) Facility. This work was financially supported by the Max Planck Society (MPG) and the Deutsche Forschungsgemeinschaft (DFG, German Research Foundation) – 1) TRR 83 (grant no. 112927078, TP23 M. Zerial) and 2) under Germany´s Excellence Strategy – EXC-2068 – 390729961– Cluster of Excellence Physics of Life of TU Dresden.

References

Ayscough K, Stryker J, Pokala N, Sanders M, Crews P, Drubin D (1997) High rates of actin filament turnover in budding yeast and roles for actin in establishment and maintenance of cell polarity revealed using the actin inhibitor latrunculin-a. J Cell Biol 137:399–416

488 Bendezü FO, Vincenzetti V, Vavylonis D, Wyss R, Vogel H, SG M (2015) Spontaneous cdc42
489 polarization independent of gdi-mediated extraction and actin-based trafficking. PLOS Biology
490 13:e1002097

491 Blümer J, Rey J, Dehmelt L, Mazel T, Wu YW, Bastiaens P, Goody RS, Itzen A (2013) Rabgefs
492 are a major determinant for specific rab membrane targeting. The Journal of Cell Biology
493 200(3):287–300. ISSN 0021-9525. doi:10.1083/jcb.201209113

494 Bos J, Rehmann H, Wittinghofer A (2007) Gefs and gaps: critical elements in the control of
495 small g proteins. Cell 129:865–877

496 Chenevert J, Corrado K, Bender A, Pringle J, I H (1992) A yeast gene (bem1) necessary for
497 cell polarization whose product contains two sh3 domains. Nature 356:77–79

498 Cherfils J, Zeghouf M (2013) Regulation of small gtpases by gefs, gaps, and gdis. Physiol Rev
499 93:269–309

500 Chiou JG, Ramirez SA, Elston TC, Witelski TP, Schaeffer DG, DJ L (2018) Principles that
501 govern competition or co-existence in rho-gtpase driven polarization. PLoS Comput Biol
502 14:e1006095

503 Christoforidis S, McBride H, Burgoyne R, Zerial M (1999a) The rab5 effector eea1 is a core
504 component of endosome docking. Nature 397:621–625

505 Christoforidis S, Miaczynska M, Ashman K, Wilm M, Zhao L, Yip S, Waterfield M, Backer J,
506 Zerial M (1999b) Phosphatidylinositol-3-oh kinases are rab5 effectors. Nat Cell Biol 1:249–
507 252

508 Delprato A, Lambright D (2007) Structural basis for rab gtpase activation by vps9 domain
509 exchange factors. Nat Struct Mol Biol 14:406–412

510 Delprato A, Merithew E, Lambright D (2004) Structure, exchange determinants, and family-
511 wide rab specificity of the tandem helical bundle and vps9 domains of rabex-5. Cell 118:607–
512 617

513 Edler E, Schulze E, M S (2017) Membrane localization and dynamics of geranylgeranylated
514 rab5 hypervariable region. Biochim Biophys Acta 1859:1335–1349

515 Edler E, Stein M (2017a) Probing the druggability of membrane-bound rab5 by molecular
516 dynamics simulations. J Enzyme Inhib Med Chem 32:434–443

517 Edler E, Stein M (2017b) Recognition and stabilization of geranylgeranylated human rab5 by
518 the gdp dissociation inhibitor (gdi). Small GTPases 0(0):1–16

519 Falasca M, Maffucci T (2012) Regulation and cellular functions of class ii phosphoinositide 3-
520 kinases. Biochem J 443:587–601

521 Farnsworth CC, Seabra MC, Ericsson LH, Gelb MH, Ja G (1994) Rab geranylgeranyl
522 transferase catalyzes the geranylgeranylation of adjacent cysteines in the small gtpases rab1a,
523 rab3a, and rab5a. Proc Natl Acad Sci USA 91:11963–11967

524 Franke C, Repnik U, Segeletz S, Brouilly N, Kalaidzidis Y, Verbavatz JM, Zerial M (2019)
525 Correlative single-molecule localization microscopy andelectron tomography reveals
526 endosome nanoscale domains. Traffic 20:601–617

527 Ghomashchi F, Zhang X, Liu L, Gelb MH (1995) Binding of prenylated and polybasic peptides
528 to membranes: affinities and intervesicle exchange. Biochemistry 34:11910–11918

529 Goryachev A, Leda M (2017) Many roads to symmetry breaking: molecular mechanisms and
530 theoretical models of yeast cell polarity. Mol Biol Cell 28:370–380

531 Goryachev AB, Leda M (2019) Autoactivation of small GTPases by the GEF-effector positive
532 feedback modules. F1000Res 2019:8

533 Goryachev A, Pokhilko A (2008) Dynamics of Cdc42 network embodies a turing-type
534 mechanism of yeast cell polarity. FEBS Lett 582:1437–1443

535 Gulli M, Jaquenoud M, Shimada Y, Niederhauser G, Wiget P, Peter M (2000) Phosphorylation
536 of the cdc42 exchange factor cdc24 by the pak-like kinase cla4 may regulate polarized growth
537 in yeast. Mol Cell 6:1155–1167

538 Halatek J, Brauns F, Frey E (2018) Self-organization principles of intracellular pattern formation. Philos
539 Trans R Soc Lond B Biol Sci 373:20170107

540 He W, Bai G, Zhou H, Wei N, White NM, Lauer J, Liu H, Shi Y, Dumitru CD, Lettieri K,
541 Shubayev V, Jordanova A, Guergueltcheva V, Griffin PR, Burgess RW, Pfaff SL, Yang XL
542 (2015) Cmt2d neuropathy is linked to the neomorphic binding activity of glycyl-trna synthetase.
543 Nature 526:710–714

544 Horiuchi H, Lippé R, McBride H, Rubino M, Woodman P, Stenmark H, Rybin V, Wilm M,
545 Ashman K, Mann M, Zerial M (1997) A novel rab5 gdp/gtp exchange factor complexed to
546 rabaptin-5 links nucleotide exchange to effector recruitment and function. Cell 90:1149–1159

547 Howell A, Savage N, Johnson S, Bose I, Wagner A, Zyla T, Nijhout H, Reed M, Goryachev A,
548 Lew D (2009) Singularity in polarization: rewiring yeast cells to make two buds. Cell 139:731–
549 743

550 Irazoqui J, Gladfelter A, Lew D (2003) Scaffold-mediated symmetry breaking by cdc42p. Nat
551 Cell Biol 5:1062–1107

552 Jacobs B, Molenaar J, patterning DESG (2019) How to stabilise cluster coexistence. PLoS One
553 14:e0213188

554 Kemphues KJ, Priess JR, Morton DG, Cheng NS. Identification of genes required for
555 cytoplasmic localization in early C. elegans embryos. Cell. 1988;52:311–320.

556 Langemeyer L, Perz A, Kümmel D, Ungermann C (2018) A guanine nucleotide exchange factor
557 (GEF) limits Rab GTPase-driven membrane fusion. J Biol Chem 293:731–739

558 Lauer J, Segeltz S, Cezanne A, Guaitoli G, Raimondi F, Gentzel M, Alva V, Habeck M,
559 Kalaidzidis Y, Ueffing M, Lupas AN, Gloeckner CJ, Zerial M (2019) Auto-regulation of Rab5

GEF activity in Rabex5 by allosteric structural changes, catalytic core dynamics and ubiquitin binding eLife 2019;8:e46302

Lebrand C, Corti M, Goodson H, *et al.* (2002) Late endosome motility depends on lipids via the small GTPase rab7. EMBO J 21:1289–1300

Lee S, Tsai YC, Mattera R, Smith WJ, Kostelansky MS, Weissman AM, Bonifacino JS, Hurley JH. (2006) Structural basis for ubiquitin recognition and autoubiquitination by Rabex-5. *Nat Struct Mol Biol*. 13:264-71

Lippe R, Horiuchi H, Runge A, Zerial M (2001) Expression, purification, and characterization of rab5 effector complex, rabaptin-5/rabex-5. Methods Enzymol 329:132–145

Mattera R, Tsai YC, Weissman AM, Bonifacino JS. 2006. The Rab5 guanine 805 nucleotide exchange factor Rabex-5 binds ubiquitin (Ub) and functions as a Ub 806 ligase through an atypical Ub interacting motif and a zinc finger domain. The 807 Journal of Biological Chemistry 281:6874-6883.

Mattera, R., & Bonifacino, J. S. (2008). Ubiquitin binding and conjugation regulate the recruitment of Rabex-5 to early endosomes. *The EMBO journal*, *27*(19), 2484–2494. doi:10.1038/emboj.2008.177

Mayne L, Kan ZY, Chetty PS, Ricciuti A, Walters BT, Englander SW (2011) Many overlapping peptides for protein hydrogen exchange experiments by the fragment separation-mass spectrometry method. J Am Soc Mass Spectrom 22:1898–1905

McBride H, Rybin V, Murphy C, Giner A, Teasdale R, Zerial M (1999) Oligomeric complexes link rab5 effectors with nsf and drive membrane fusion via interactions between eea1 and syntaxin 13. Cell 98:377– 386

Motegi, F., & Seydoux, G. (2013). The PAR network: redundancy and robustness in a symmetry-breaking system. Philosophical transactions of the Royal Society of London. Series B, Biological sciences, 368(1629), 20130010. doi:10.1098/rstb.2013.0010

Murray J, Panaretou C, Stenmark H, Miaczynska M, Backer J (2002) Role of rab5 in the recruitment of hvps34/p150 to the early endosome. Traffic 3:416–427

Münzberg E, Stein M (2019) Structure and Dynamics of Mono- vs. Doubly Lipidated Rab5 in Membranes. Int J Mol Sci 20, 4773.

Nagashima Y, Tsugawa S, Mochizuki A, Sasaki T, Fukuda H, Oda Y (2018) A rho-based reaction-diffusion system governs cell wall patterning in metaxylem vessels. Scientific Reports 8:11542

Neumann S, Pucadyil T, Schmid S (2013) Analyzing membrane remodeling and fission using supported bilayers with excess membrane reservoir. Nature Protocols 8:213–222

Oda Y, Fukuda H (2012) Initiation of cell wall pattern by a rho- and microtubule-driven symmetry breaking. Science 337(6100):1333–1336. ISSN 0036-8075. doi:10.1126/science.1222597

600 Penengo L, Mapelli M, Murachelli A, Confalonieri S, Magri L, Musacchio A, Di Fiore P, Polo
601 S, Schneider T (2006) Crystal structure of the ubiquitin binding domains of rabex-5 reveals two
602 modes of interaction with ubiquitin. Cell 124:1183–1195

603 Perini E (2012) In vitro reconstitution of the molecular mechanisms of vesicle tethering and
604 membrane fusion. Ph.D. thesis, MPI-CBG, Dresden

605 Pylypenko O, Rak A, Durek T, Kushnir S, Dursina BE, Thomae NH, Constantinescu AT,
606 Brunsveld L, Watzke A, Waldmann H, Goody RS, Alexandrov K (2006) Structure of doubly
607 prenylated ypt gdi complex and the mechanism of gdi-mediated rab recycling. EMBO J 25:13–
608 23

609 Rak A, Pylypenko O, Niculae A, Pyatkov K, Goody RS, Alexandrov K (2004) Structure of the
610 rab7: Rep-1 complex: Insights into the mechanism of rab prenylation and choroideremia
611 disease. Cell 117:749–760

612 Rizk A, Paul G, Incardona P, Bugarski M, Mansouri M, Niemann A, Ziegler U, Berger P,
613 Sbalzarini IF (2014) Segmentation and quantification of subcellular structures in fluorescence
614 microscopy images using Squassh. Nature Protocols 9(3):586–596

615 Sasaki T, Kikuchi A, Araki S, Hata Y, Isomura M, Kuroda S, and TYP (1990) and
616 characterization from bovine brain cytosol of a protein that inhibits the dissociation of gdp from
617 and the subsequent binding of gtp to smg p25a, a ras p21-like gtp-binding protein. J Biol Chem
618 265:2333–2337

619 Schindelin, J.; Arganda-Carreras, I. & Frise, E. et al. (2012), "Fiji: an open-source platform for
620 biological-image analysis", *Nature methods* **9(7)**: 676-682,

621 Semerdjieva S, Shortt B, Maxwell E, Singh S, Fonarev P, Hansen J, Schiavo G, Grant B,
622 Smythe E (2008) Coordinated regulation of ap2 uncoating from clathrin-coated vesicles by rab5
623 and hrme-6. J Cell Biol 183:499–511

624 Snyder, JP and U. S. Government Printing Office, “Map projections: A working manual,” Tech.
625 Rep., Washington, D.C., 1987.

626 Stenmark H, Vitale G, Ullrich O, Zerial M (1995) Rabaptin-5 is a direct effector of the small
627 gtpase rab5 in endocytic membrane fusion. Cell 83:423–432

628 Sternberg, “Biomedical image processing,” Computer, vol. 16, no. 1, pp. 22–34, Jan 1983.

629 Snyder, JP and U. S. Government Printing Office, “Map projections: A working manual,” Tech.
630 Rep., Washington, D.C., 1987.

631 Sönnichsen B, De Renzis S, Nielsen E, Rietdorf J, Zerial M (2000) Distinct membrane domains
632 on endosomes in the recycling pathway visualized by multicolor imaging of rab4, rab5, and
633 rab11. J Cell Biol 149(4):901–914

634 Tall GG, Barbieri MA, Stahl PD, Horazdovsky BF (2001) Ras-activated endocytosis is
635 mediated by the rab5 guanine nucleotide exchange activity of rin1. Developmental Cell 1:73–
636 82

637 Turing AM (1952) The chemical basis of morphogenesis. Phil Trans R Soc Lond B 237, 37-72

638 Walters BT, Ricciuti A, Mayne L, Englander SW (2012) Minimizing back exchange in the
639 hydrogen exchange-mass spectrometry experiment. J Am Soc Mass Spectrom 23:2132–2139

640 Wang M, Casey P (2016) Protein prenylation: unique fats make their mark on biology. Nature
641 Reviews Molecular Cell Biology 17:110 EP –

642 Woods B, Lew DJ (2019) Polarity establishment by cdc42: Key roles for positive feedback and
643 differential mobility. Small GTPases 10:130–137

644 Wu YW, Oesterlin LK, Tan KT, Waldmann H, Alexandrov K, Rs G (2010) Membrane targeting
645 mechanism of rab gtpases elucidated by semisynthetic protein probes. Nat Chem Biol 6:534–
646 540

647 Yang Z, Lavagi I (2012) Spatial control of plasma membrane domains: Rop gtpase-based
648 symmetry breaking. Curr Opin Plant Biol 15:601–607

649 Zhang Z, Zhang T, Wang S, Gong Z, Tang C, Chen J, Ding J (2014) Molecular mechanism for
650 rabex-5 gef activation by rabaptin-5. Elife 3

651 Zhou Y, Prakash P, Liang H, Cho KJ, Gorfe AA, Jf H (2017) Lipid-sorting specificity encoded
652 in k-ras membrane anchor regulates signal output. Cell 168:239–251

653 Zhu H, Zhu G, Liu J, Liang Z, Zhang X, Li G (2007) Rabaptin-5-independent membrane
654 targeting and rab5 activation by rabex-5 in the cell. Mol Biol Cell 18:4119–4128
655
656 Zerial, M., McBride, H. (2001) Rab proteins as membrane organizers. *Nat Rev Mol Cell*
657 *Biol* **2,** 107–117

658

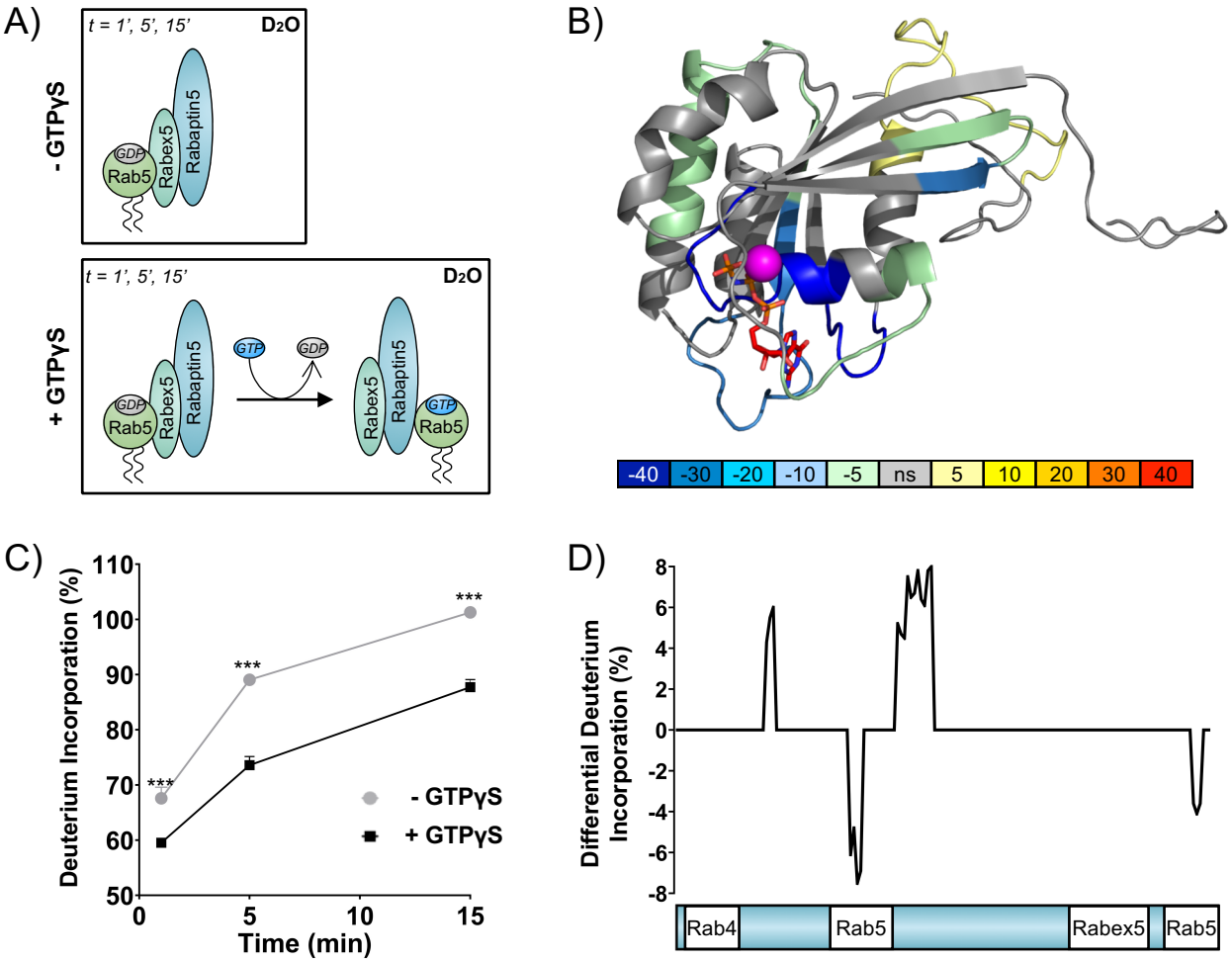

Figure 1: **Rab5 backbone dynamics during nucleotide exchange. A** Scheme of reaction. The ternary complex (Rab5/Rabex5/Rabaptin5) was incubated in D_2O for 1, 5 or 15 minutes in the presence or absence of GTPγS. **B** Crystal structure of Rab5:GTP (PDBID: 3MJH) pseudocolored to show differential uptake of ternary complex (Rab5/Rabex5/Rabaptin5) ± GTPγS (average of 1min, 5min & 15min timepoints). The Mg^{2+} ion is shown as a sphere (magenta) and GTPγS as a line structure. Color scheme: regions that are protected from exchange, i.e. stabilization, are colored with cool colors; regions with enhanced exchange with warm colors; regions with no statistically different uptake are colored in grey; and regions with no peptide coverage are white. **C** Deuterium incorporation over time in Rab5 β2 (aa 58-63, colored blue in **B**, in the ternary complex (Rab5/Rabex5/Rabaptin5) ± GTPγS **D** Differential deuterium incorporation in Rabaptin5 during the nucleotide exchange reaction. Two areas of protection (decrease in deuterium uptake) correspond with the Rab5 binding sites.

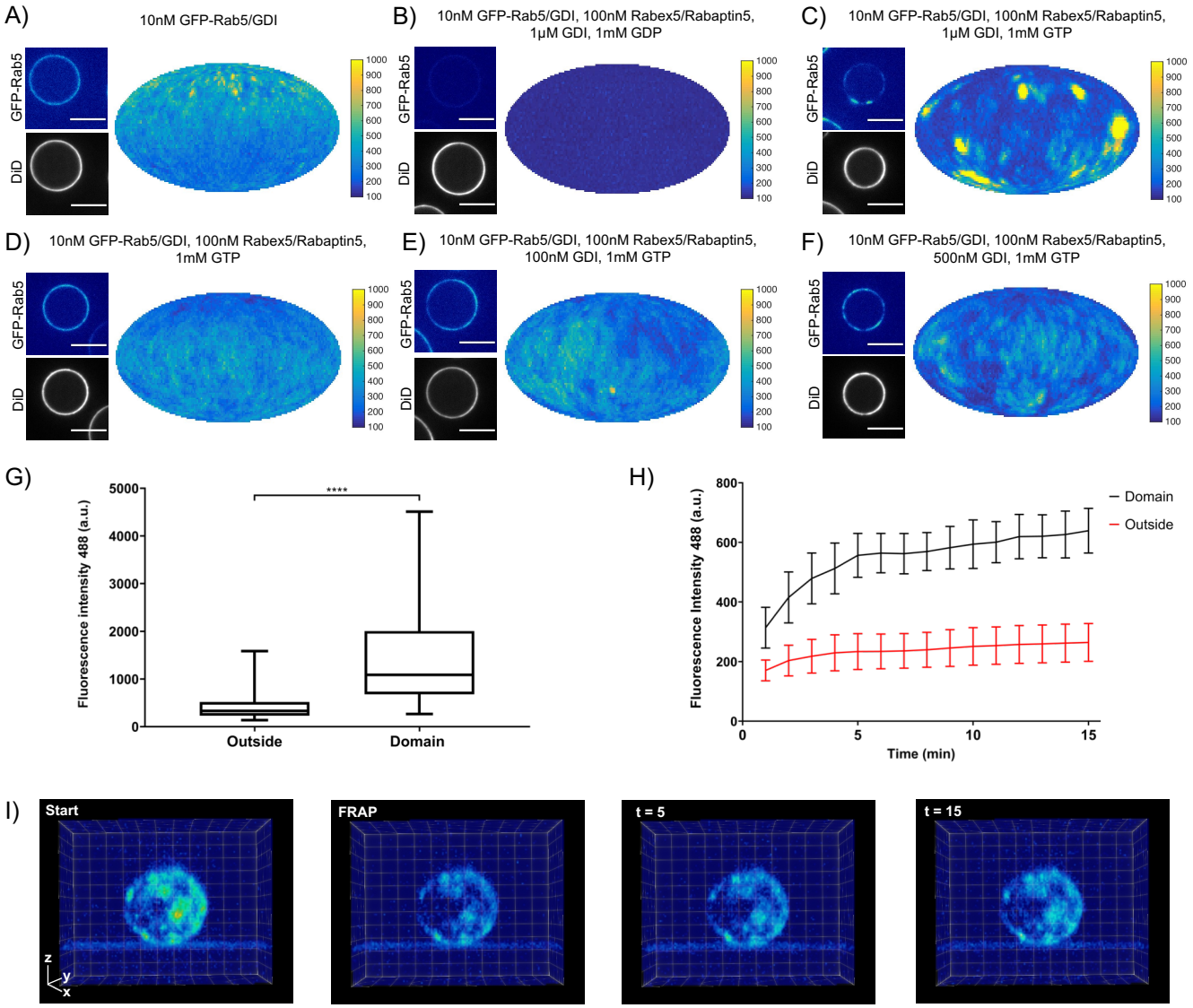

Figure 2: **Rab5 domains can be reconstituted *in vitro*.** EE MCBs were incubated for 15 minutes at 23˚C with 10nM GFP-Rab5/GDI **A** and supplemented with 1µM GDI, 100nM Rabex5/Rabaptin5-RFP and 1mM GDP (**B**) or GTP (**C**). **D-F** GDI is necessary for Rab5 domain formation. EE MCBs were incubated with 10nM GFP-Rab5/GDI complex**,** 100nM Rabex5/Rabaptin5 1mM GTP and 0nM (**D**), 100nM (**E**) or 500nM (**F**) GDI. Beads are presented as equatorial slices in GFP and DiD channels (*left*) and a Mollweide projection of the GFP channel (*right*). Scale Bar = 10µm. **G** Mean GFP-Rab5 signal intensity outside of and within segmented domains in **C** (See also Table 1) (p= <0.0001) **H** EE MCBs were at 23˚C with 10nM GFP-Rab5/GDI 1µM GDI, 100nM Rabex5/Rabaptin5 and 1mM GTP and imaged in 1 minute intervals for a total of 15 minutes. Graph presents mean GFP-Rab5 signal intensity outside of and within segmented domains over time (n = 63). **I** EE MCBs were incubated for 15 minutes at 23˚C with 10nM GFP-Rab5/GDI 1µM GDI, 100nM Rabex5/Rabaptin5 and 1mM GTP (*panel 1*; ‚Start') then bleached (*panel 2*; ‚FRAP') and imaged in 1 minute intervals for a total of 15 minutes (Shown here are stills from Video 2)

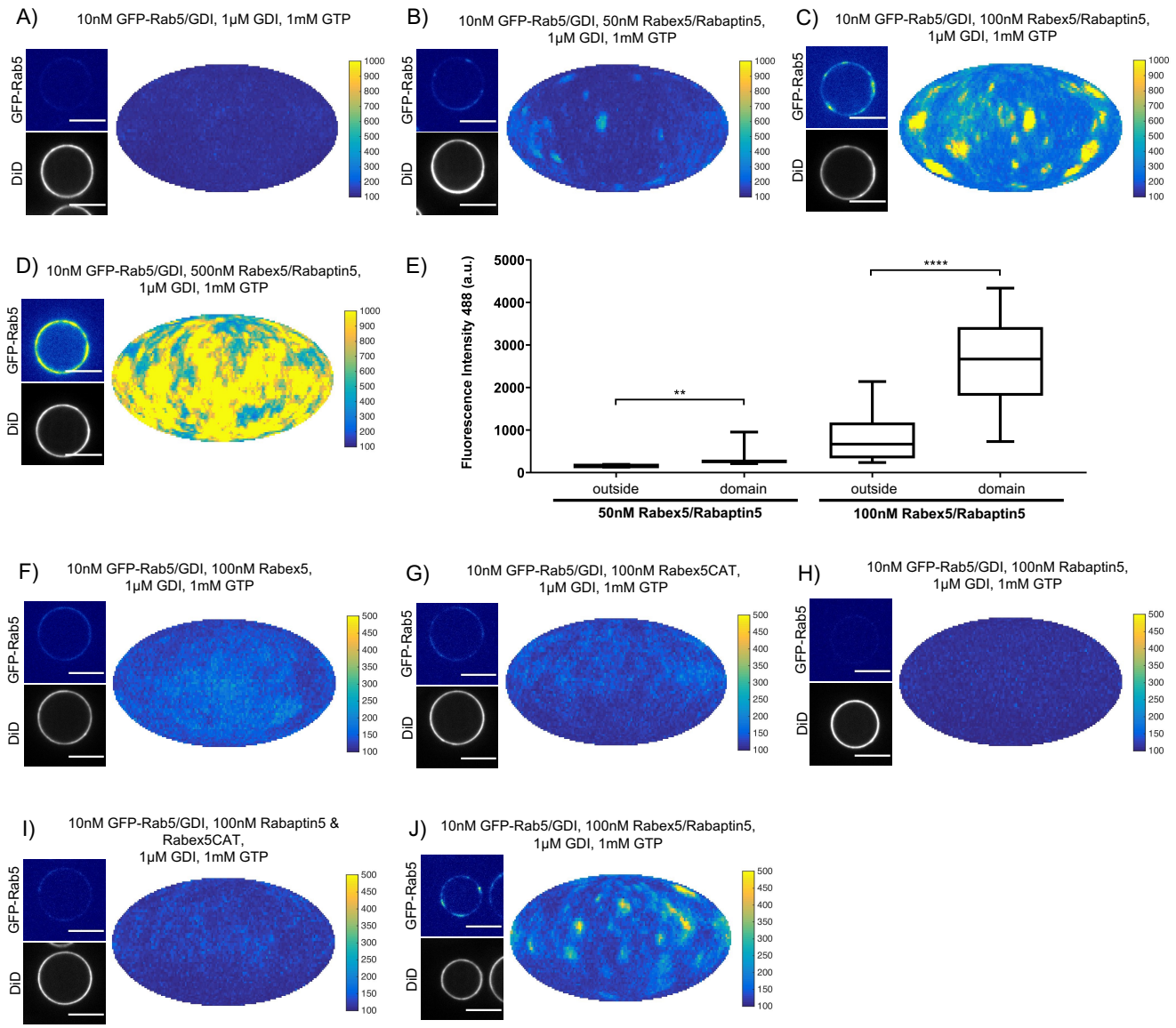

Figure 3: **Rabex5/Rabaptin5 is essential for Rab5 domain formation in vitro. A - E** Domain formation is dependent on concentration of Rabex5/Rabaptin5. EE MCBs were incubated for 15 minutes at 23˚C with 10nM GFP-Rab5/GDI, 1μM GDI, 1mM GTP and 0nM (**A**), 50nM (**B**), 100nM (**C**), or 500nM (**D**) Rabex5/Rabaptin5-RFP. (**E**) Mean GFP-Rab5 signal intensity outside of and within segmented domains as a function of Rabex5/Rabaptin5 concentration (50nM Rabex5/Rabaptin5 p=0.001; 100nM Rabex5/Rabaptin5 p= <0.0001) See also Table 2) **F - J** Rabex5/Rabaptin5 cannot be split into component parts and still form domains. EE MCBs were incubated for 15 minutes at 23˚C with 10nM GFP-Rab5/GDI, 1μM GDI, 1mM GTP and 100nM Rabex (**F**), 100nM RabexCAT (**G**), 100nM Rabaptin5 (**H**), 100nM Rabex5CAT and Rabaptin5 (**I**), or 100nM Rabex5/Rabaptin5 (**J**). Beads are presented as equatorial slices in GFP and DiD channels (*left*) and a Mollweide projection of the GFP channel (*right*). Scale Bar = 10μm.

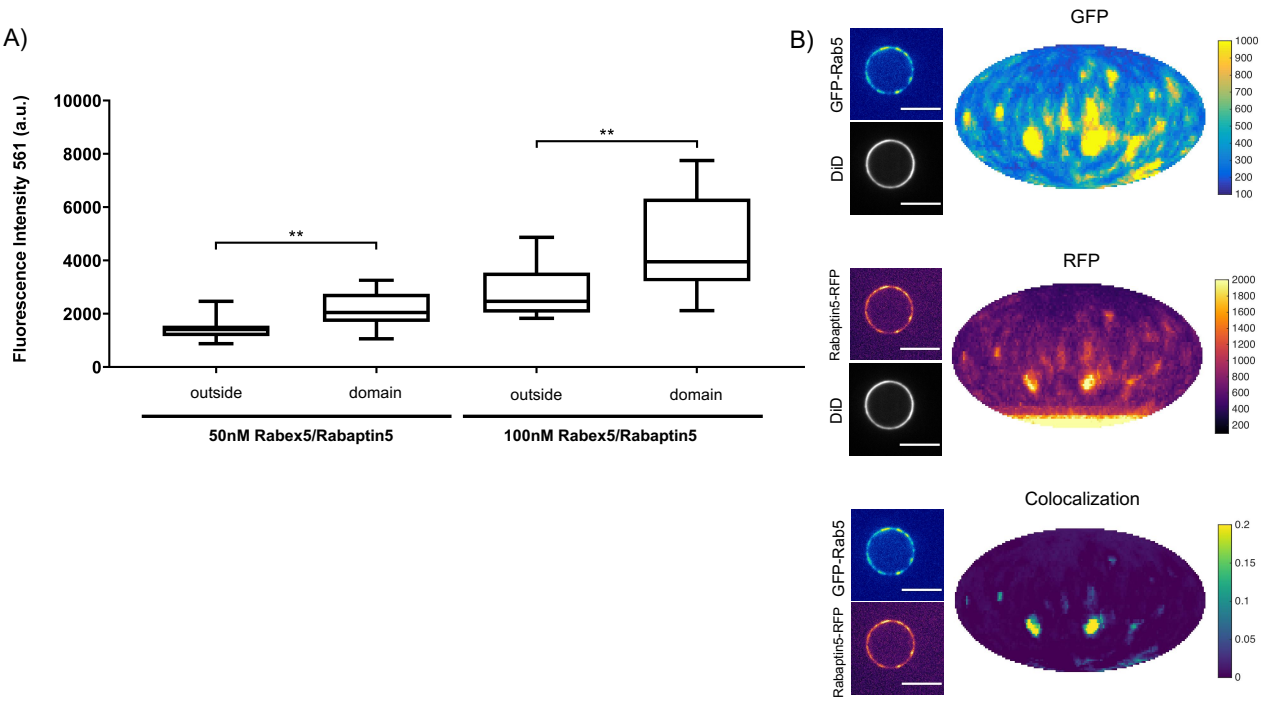

Figure 4: **Rabex5/Rabaptin5 localises to the reconstituted Rab5 domain.** EE MCBs were incubated for 15 minutes at 23˚C with 10nM GFP-Rab5/GDI, 1μM GDI, 1mM GTP and 50nM or 100nM Rabex5/Rabaptin5-RFP (See Figure 3 A-E). **A** Rabaptin5-RFP signal is enriched in domains. (50nM Rabaex5/Rabaptin5 p=0.001; 100nM Rabex5/Rabaptin5 p= 0.0017). Corresponding GFP enrichment in presented in Figure 3 E. **B** Equatorial slices and mollweide representations of GFP signal (*top*), RFP signal (*bottom*) and pixelwise GFP-RFP colocalization (*bottom*). Beads are presented as equatorial slices (*left*) and Mollweide projections (*right*). Scale Bar = 10μm.

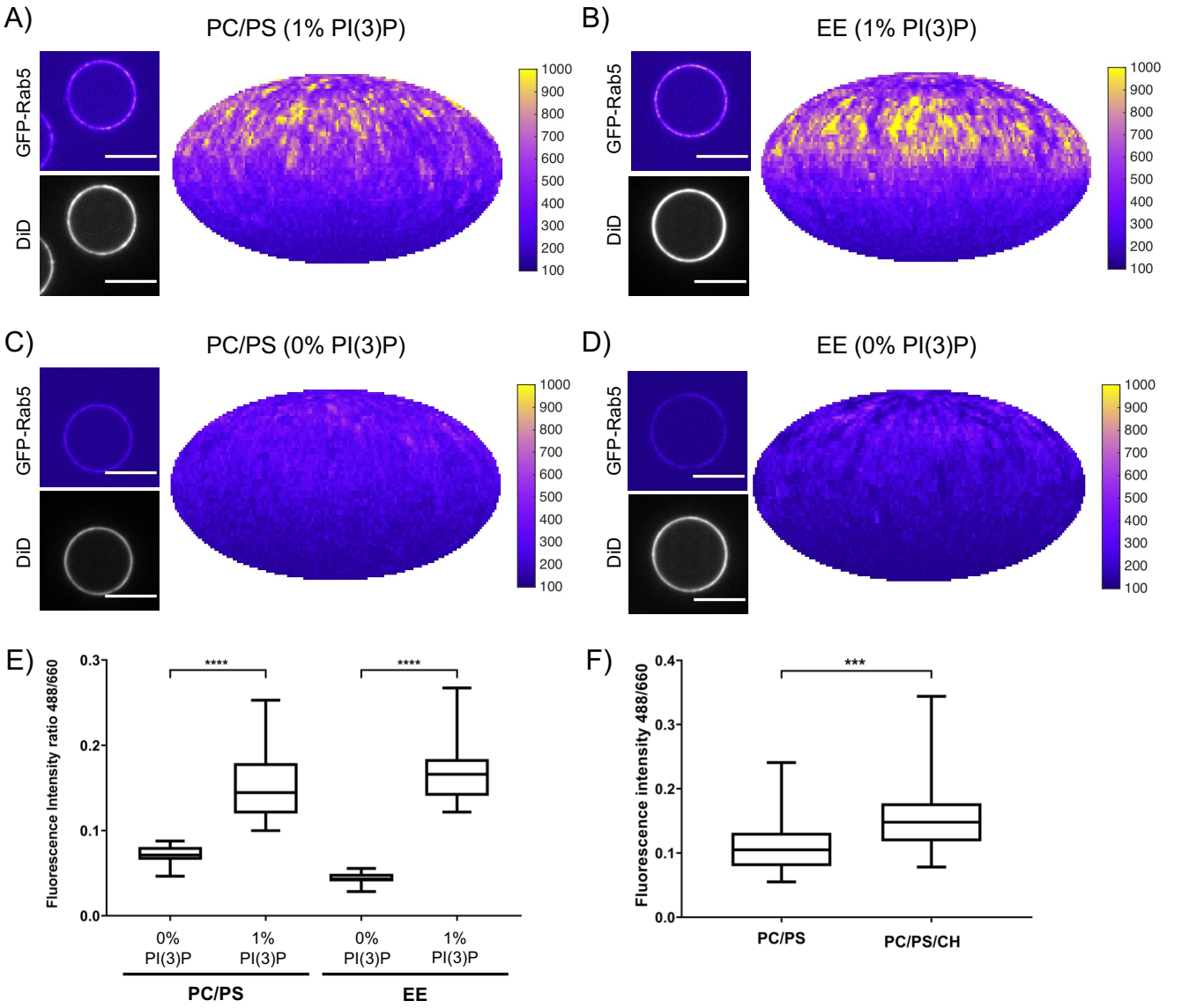

Figure 5: **Recruitment of geranylgeranylated GFP-Rab5 to EE and PC/PS bilayers is enhanced by PI(3)P.** MCBs with PC/PS and EE lipid composition containing 1mol% PI(3)P (**A** and **B** respectively) and MCBs with PC/PS and EE lipid composition containing 0mol% PI(3)P (**C** and **D** respectively) were incubated with 10nM GFP-Rab5/GDI for 15 minutes at 23˚C. Beads are presented as equatorial slices in GFP and DiD channels (*left*) and Mollweide projection of the GFP channel (*right*). Scale Bar = 10μm. **E** Mean equatorial GFP signal intensity in **A-D**. (p=<0.0001) **F** MCBs with PC/PS and PC/PS/CH lipid composition (0mol% PI(3)P) incubated with 10nM GFP-Rab5/GDI for 15 minutes at 23˚C. Graph presents mean equatorial GFP signal intensity (p=0.005). For both **E** and **F** GFP signal intensity is normalized to DiD signal intensity, however the same pattern can be seen in the raw intensity values.

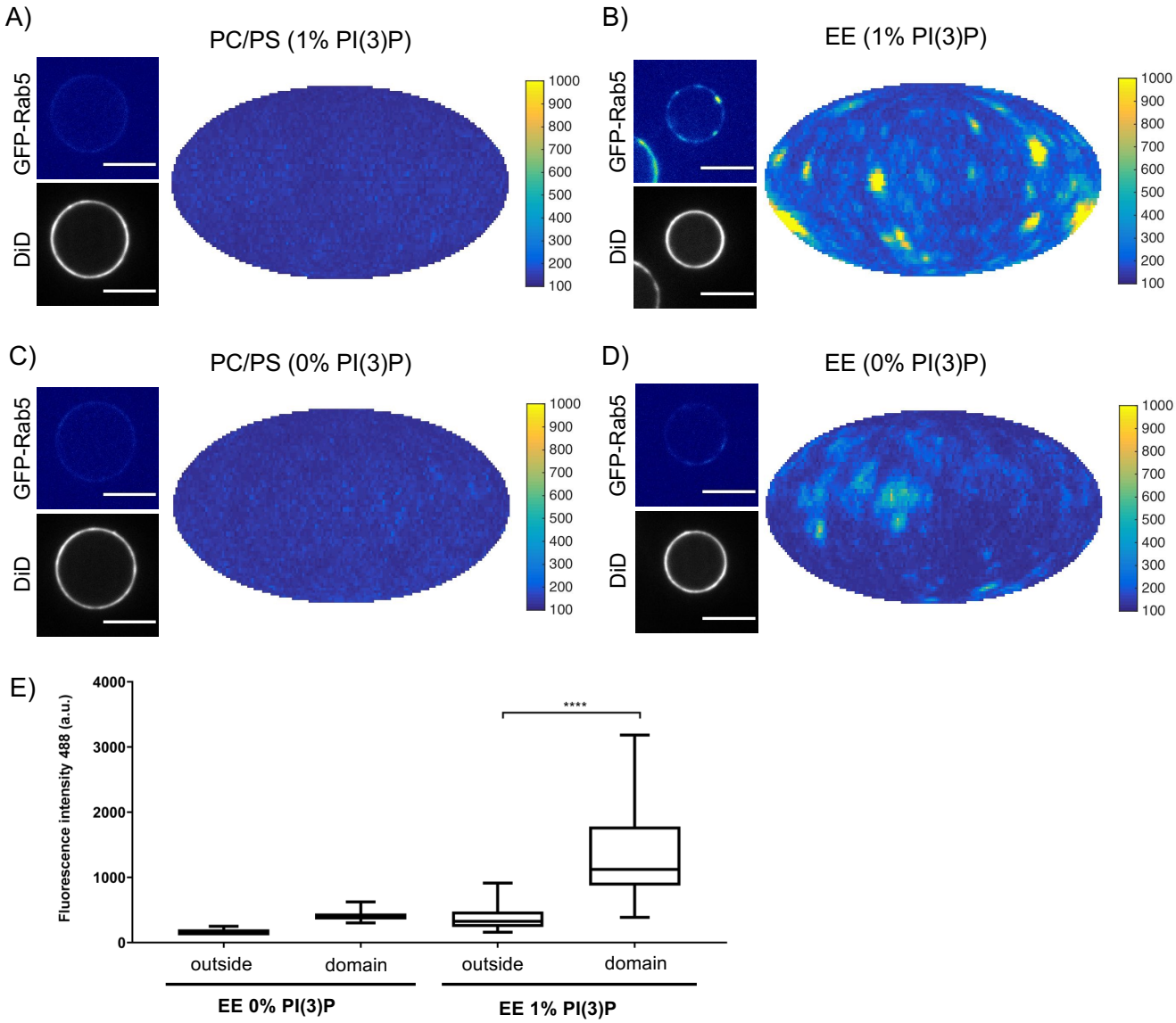

Figure 6: **Rab5 domain formation in vitro is influenced by membrane composition.** MCBs with PC/PS and EE lipid composition containing 1mol% PI(3)P (**A** and **B** respectively) and MCBs with PC/PS and EE lipid composition containing 0mol% PI(3)P (**C** and **D** respectively) were incubated with 10nM GFP-Rab5/GDI, 1μM GDI, 100nM Rabex5/Rabaptin5-RFP and 1mM GTP for 15 minutes at 23˚C. Beads are presented as equatorial slices in GFP and DiD channels (*left*) and Mollweide projection of the GFP channel (*right*). Scale Bar = 10μm. **E** Mean GFP-Rab5 signal intensity outside of and within segmented domains in **B** and **D (p=<0.0001)** (See also Table 1).

	10nM GFP-Rab5/GDI	**10nM GFP-Rab5/GDI, 100nM Rabex5/Rabaptin5, 1µM GDI, 1mM GDP**	**10nM GFP-Rab5/GDI, 100nM Rabex5/Rabaptin5, 1µM GDI, 1mM GTP**
# Domains	0	0	449
# Beads	30	44	96
Mean # Domains/Bead	0	0	4.7
Mean intensity/Bead (a.u.)	212.31 ± 67.04	128.40 ± 4.91	447.96 ± 403.41
Mean Standard Deviation/Bead	46.70 ± 21.26	0.36 ± 0.04	237.24 ± 225.54
Mean Intensity/Domain	-	-	1326.95 ± 1026.96
Mean Intensity/Outside	262.68 ± 42.58	128.40 ± 4.91	454.63 ± 364.79
Mean domain area, μm^2	-	-	$1.74^{+4.74}_{-1.00}$
Mean domain diameter, μm	-	-	1.32

Table 1 **Rab5 domains can be reconstituted *in vitro*.** EE MCBs were incubated for 15 minutes at 23˚C with 10nM GFP-Rab5/GDI and supplemented with 1µM GDI, 100nM Rabex5/Rabaptin5-RFP and 1mM GDP or GTP.

	10nM GFP-Rab5/GDI, 1µM GDI, 1mM GTP	**10nM GFP-Rab5/GDI, 50nM Rabex5/Rabaptin5, 1µM GDI, 1mM GTP**	**10nM GFP-Rab5/GDI, 100nM Rabex5/Rabaptin5, 1µM GDI, 1mM GTP**
# Domains	0	96	90
# Beads	17	23	16
Mean # Domains/Bead	0	4.17	5.63
Mean intensity/Bead (a.u.)	132.95 ± 6.23	164.66 ± 24.13	946.76 ± 669.27
Mean Standard Deviation/Bead	13.14 ± 2.68	41.63 ± 17.87	526.77 ± 332.23
Mean Intensity/Domain	-	282.58 ± 96.68	2767.14 ± 1039.34
Mean Intensity/Outside	132.95 ± 6.23	158.82 ± 20.73	856.22 ± 573.11
Mean domain area, μm^2	-	$^{+\ 3.36}_{1.71-\ 0.95}$	$^{+\ 6.22}_{1.97\ -\ 1.26}$
Mean domain diameter, μm	-	1.31	1.40

Table 2 **Domain formation is dependent on concentration of Rabex5/Rabaptin5.** EE MCBs were incubated for 15 minutes at 23˚C with 10nM GFP-Rab5/GDI, 1µM GDI, 1mM GTP and 0nM, 50nM, 100nM Rabex5/Rabaptin5-RFP. Beads incubated with 10nM GFP-Rab5/GDI, 1µM GDI, 1mM GTP and 500nM Rabex5/Rabaptin5-RFP could not be properly segmented due to the high GFP-Rab5 signal on the bead (See Figure 3 D).

	PC/PS (0% PI(3)P)	PC/PS (1% PI(3)P)	EE (0% PI(3)P)	EE (1% PI(3)P)
# Domains	0	0	13	164
# Beads	33	38	24	40
Mean # Domains/Bead	0	0	0.54	4.1
Mean intensity/Bead (a.u.)	135.48 ± 14.69	129.54 ± 11.79	138.06 ± 36.91	429.23 ± 217.66
Mean Standard Deviation/Bead	16.69 ± 8.60	13.23 ± 6.02	26.05 ± 25.50	245.40 ± 120.62
Mean Intensity/Domain	-	-	508.32 ± 143.37	1269.32 ± 556.54
Mean Intensity/Outside	135.48 ± 14.69	129.54 ± 11.79	192.10 ± 72.51	393.35 ± 194.66
Mean domain area, μm^2	-	-	$2.12^{+4.76}_{-1.21}$	$1.42^{+2.67}_{-0.73}$
Mean domain diameter, μm	-	-	1.46	1.19

Table 3 **Rab5 domain formation in vitro is influenced by membrane composition**. MCBs with EE and PC/PS lipid composition containing 1mol% PI(3)P and MCBs with EE and PC/PS lipid composition containing 0mol% PI(3)P were incubated with 10nM GFP-Rab5/GDI, 1µM GDI, 100nM Rabex5/Rabaptin5-RFP and 1mM GTP for 15 minutes at 23˚C.

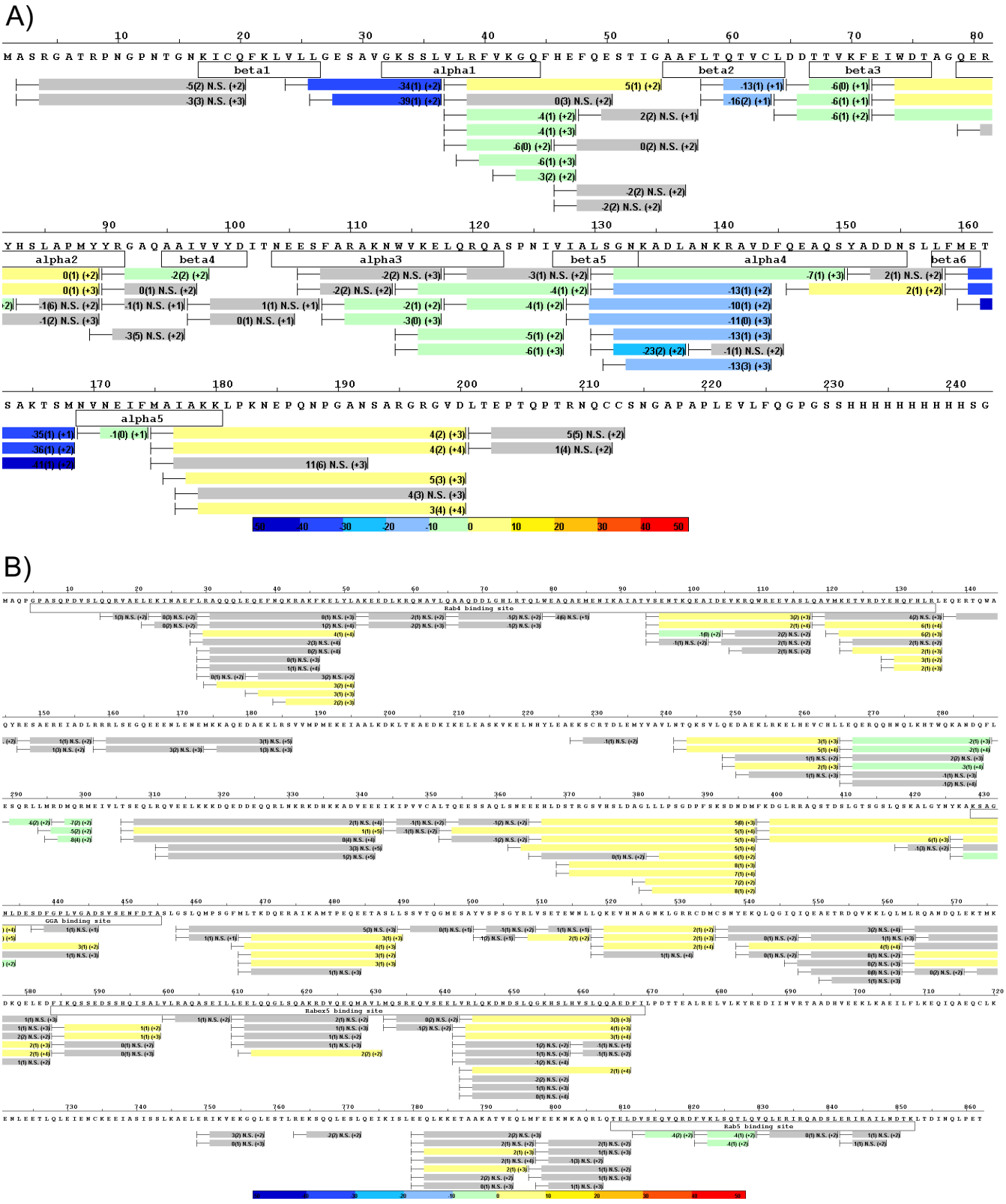

Supplement to Figure 1: **HDX data for Rab5 and Rabaptin5 backbone dynamics during nucleotide exchange. A** Differential uptake of Rab5 in the ternary complex (Rab5/Rabex5/Rabaptin5) ± GTPγS (average of 1min, 5min & 15min timepoints). See also Figure 1 B. **B** Differential uptake of Rabaptin5 in the ternary complex (Rab5/Rabex5/Rabaptin5) ± GTPγS (average of 1min, 5min & 15min timepoints). See also Figure 1 D.

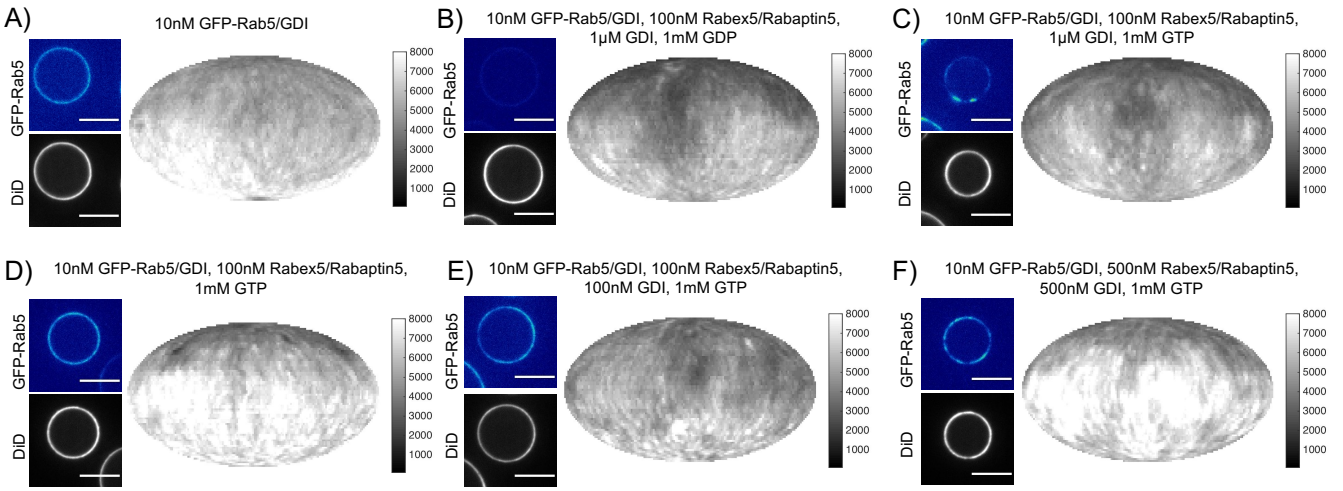

Supplement to Figure 2: **Rab5 domains can be reconstituted *in vitro*.** EE MCBs were incubated for 15 minutes at 23˚C with 10nM GFP-Rab5/GDI **A** and supplemented with 1μM GDI, 100nM Rabex5/Rabaptin5-RFP and 1mM GDP (**B**) or GTP (**C**). **D-F** GDI is for Rab5 domain formation. EE MCBs were incubated with 10nM GFP-Rab5/GDI complex**,** 100nM Rabex5/Rabaptin5 1mM GTP and 0nM (**D**), 100nM (**E**) or 500nM (**F**) GDI. Beads are presented as equatorial slices in GFP and DiD channels (*left*) and Mollweide projection of the DiD channel (*right*).

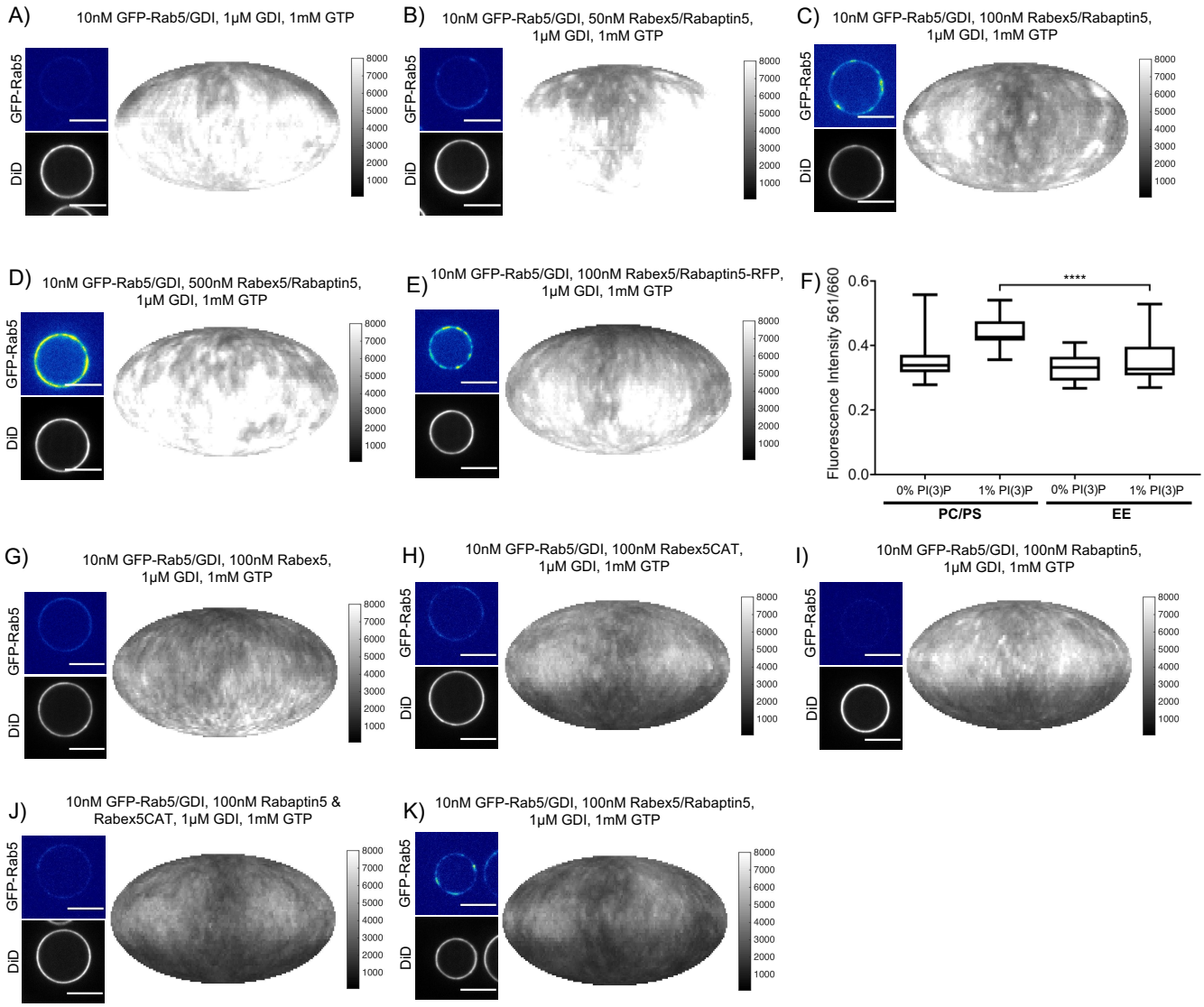

Supplement to Figure 3: **Rabex5/Rabaptin5 is essential for Rab5 domain formation in vitro**. **A - E** Domain formation is dependent on concentration of Rabex5/Rabaptin5. EE MCBs were incubated for 15 minutes at 23˚C with 10nM GFP-Rab5/GDI, 1μM GDI, 1mM GTP and 0nM (**A**), 50nM (**B**), 100nM (**C** & **E**; (**E**) MCB shown for GFP/RFP colocalization in Figure 3 F), or 500nM (**D**) Rabex5/Rabaptin5-RFP. **F** Mean equatorial RFP intensity of MCBs of different lipid compositions (See Supplemental Table 1) incubated for 15 minutes at 23˚C with 100nM Rabex5/Rabaptin5-RFP. (p= <0.0001) **G-K** Rabex5/Rabaptin5 cannot be split into component parts and still form domains. EE MCBs were incubated for 15 minutes at 23˚C with 10nM GFP-Rab5/GDI, 1μM GDI, 1mM GTP and 100nM Rabex (**G**), 100nM RabexCAT (**H**), 100nM Rabaptin5 (**I**), 100nM Rabaptin5 and Rabex5CAT (**J**), or 100nM Rabex5/Rabaptin5 (**K**). Beads are presented as equatorial slices in GFP and DiD channels (*left*) and Mollweide projection of the DiD channel (*right*). Scale Bar = 10μm.

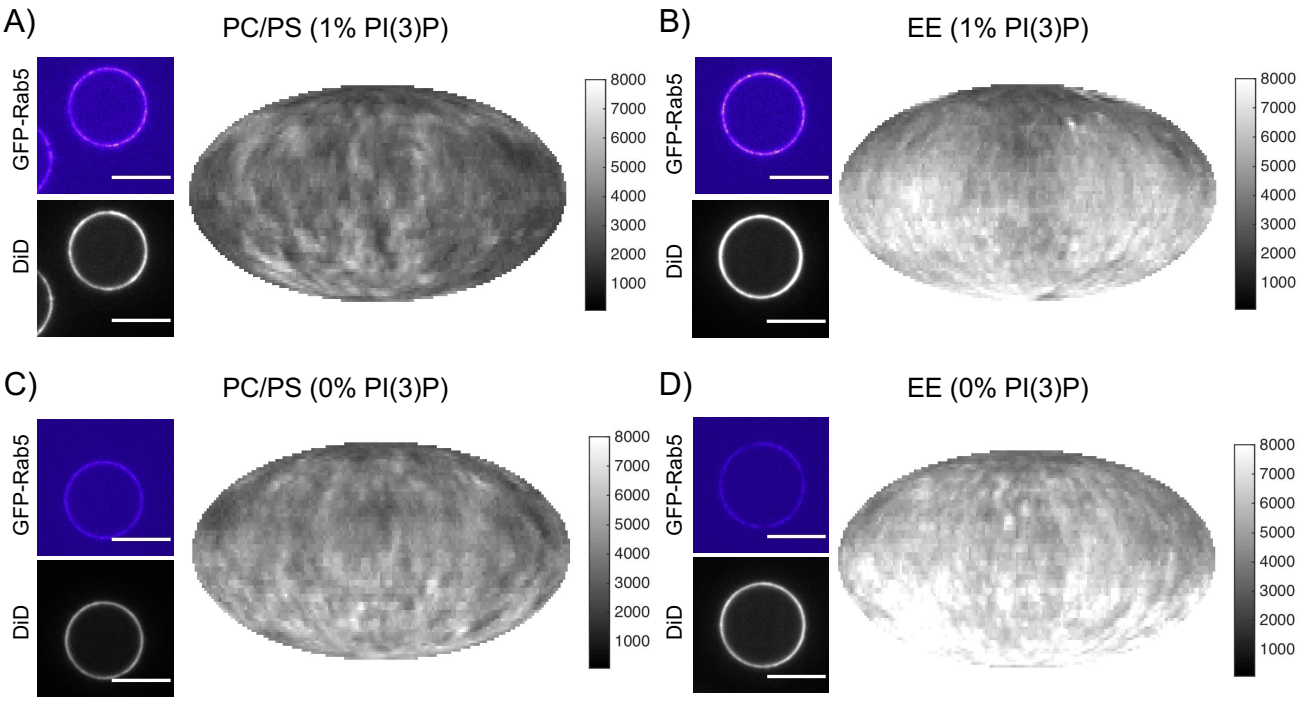

Supplement to Figure 5: **Recruitment of geranygeranylated GFP-Rab5 to EE and PC/PS bilayers is enhanced by PI(3)P.** MCBs with PC/PS and EE lipid composition containing 1mol% PI(3)P (**A** and **B** respectively) and MCBs with PC/PS and EE lipid composition containing 0mol% PI(3)P (**C** and **D** respectively) were incubated with 10nM GFP-Rab5/GDI for 15 minutes at 23˚C. Beads are presented as equatorial slices in GFP and DiD channels (*left*) and Mollweide projection of the DiD channel (*right*). Scale Bar = 10μm.

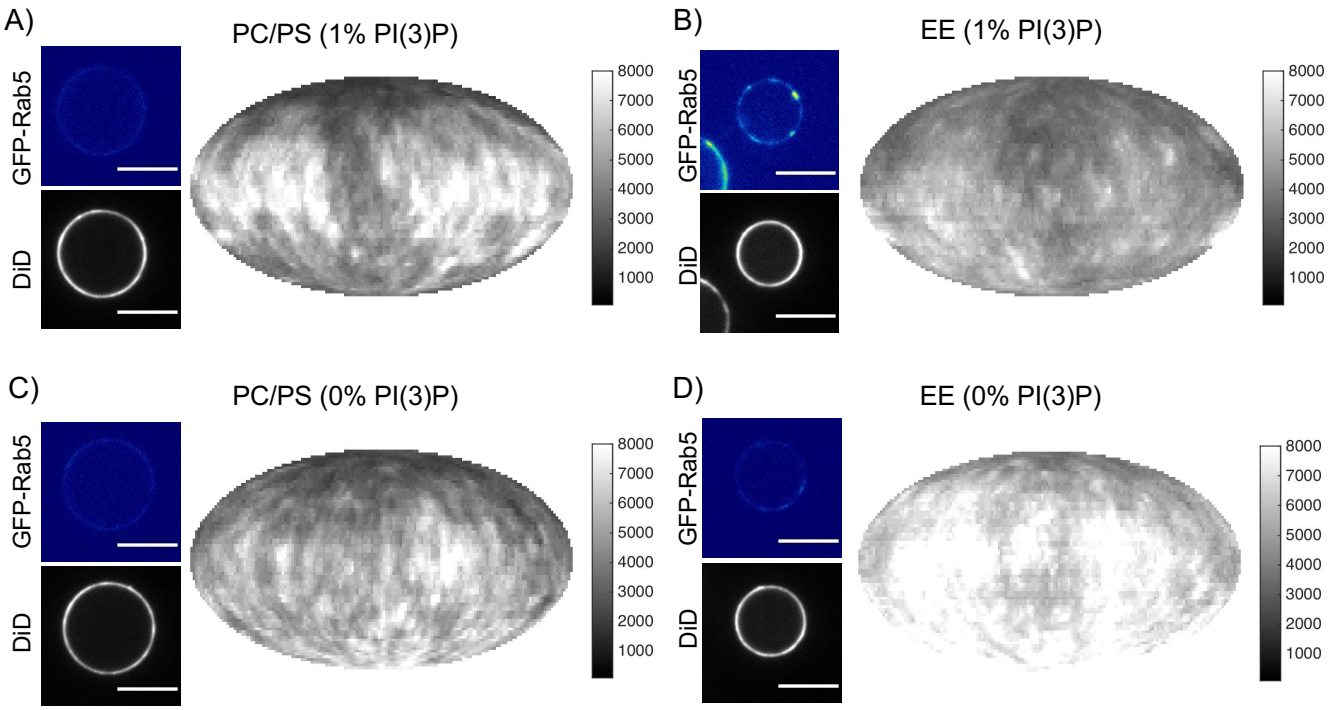

Supplement to Figure 6**: Rab5 domain formation in vitro is influenced by membrane composition.** MCBs with PC/PS and EE lipid composition containing 1mol% PI(3)P (**A** and **B** respectively) and MCBs with PC/PS and EE lipid composition containing 0mol% PI(3)P (**C** and **D** respectively) were incubated with 10nM GFP-Rab5/GDI, 1μM GDI, 100nM Rabex5/Rabaptin5-RFP and 1mM GTP for 15 minutes at 23˚C. Beads are presented as equatorial slices in GFP and DiD channels (*left*) and Mollweide projection of the DiD channel (*right*). Scale Bar = 10μm.

	EE-MCB (mol%)	**PC/PS/CH-MCB (mol%)**	**PC/PS-MCB (mol%)**
Cholesterol	32.2	32.2	-
DOPC	16.6/15.6	51.7	84.9/83.9
Plasmalogen PE	12.9	-	-
Sphingomyelin	12.6	-	-
GM3	9	-	-
DOPS	6.1	15	15
DOPE	6.8	-	-
Plasmalogen PC	3.6	-	-
PI(3)P	0/1	-	0/1
DiD	0.1	0.1	0.1

Supplemental Table 1. **Lipid compositions used in this study.**